A Section 508–conformant HTML version of this article is available at https://doi.org/10.1289/EHP11690.

Tracking Targets of Dynamic Super-Enhancers *in Vitro* to Better Characterize Osteoclastogenesis and to Evaluate the Effect of Diuron on the Maturation of Human Bone Cells

Robel A. Tesfaye,[1,3,4] Melanie Lavaud,[1]* Céline Charrier,[1] Bénédicte Brounais-Le Royer,[1] Pierre-François Cartron,[1,2,3,4] Franck Verrecchia,[1] Marc Baud'huin,[1] François Lamoureux,[1] Steven Georges,[1]* and Benjamin Ory[1,3,4]**

[1]CRCI2NA, INSERM UMR 1307, CNRS UMR 6075, Nantes University and Angers University, Nantes, France
[2]LaBCT, Institut de Cancérologie de l'Ouest, Saint Herblain, France
[3]Cancéropole Grand-Ouest, réseau Epigénétique, Nantes, France
[4]EpiSAVMEN, Epigenetic consortium Pays de la Loire, France

Background: Osteoclasts are major actors in the maintenance of bone homeostasis. The full functional maturation of osteoclasts from monocyte lineage cells is essential for the degradation of old/damaged bone matrix. Diuron is one of the most frequently encountered herbicides, particularly in water sources. However, despite a reported delayed ossification *in vivo*, its impact on bone cells remains largely unknown.

Objectives: The objectives of this study were to first better characterize osteoclastogenesis by identifying genes that drive the differentiation of $CD14^+$ monocyte progenitors into osteoclasts and to evaluate the toxicity of diuron on osteoblastic and osteoclastic differentiation *in vitro*.

Methods: We performed chromatin immunoprecipitation (ChIP) against H3K27ac followed by ChIP-sequencing (ChIP-Seq) and RNA-sequencing (RNA-Seq) at different stages of differentiation of $CD14^+$ monocytes into active osteoclasts. Differentially activated super-enhancers and their potential target genes were identified. Then to evaluate the toxicity of diuron on osteoblasts and osteoclasts, we performed RNA-Seq and functional tests during *in vitro* osteoblastic and osteoclastic differentiation by exposing cells to different concentrations of diuron.

Results: The combinatorial study of the epigenetic and transcriptional remodeling taking place during differentiation has revealed a very dynamic epigenetic profile that supports the expression of genes vital for osteoclast differentiation and function. In total, we identified 122 genes induced by dynamic super-enhancers at late days. Our data suggest that high concentration of diuron (50 μM) affects viability of mesenchymal stem cells (MSCs) *in vitro* associated with a decrease of bone mineralization. At a lower concentration (1 μM), an inhibitory effect was observed *in vitro* on the number of osteoclasts derived from $CD14^+$ monocytes without affecting cell viability. Among the diuron-affected genes, our analysis suggests a significant enrichment of genes targeted by pro-differentiation super-enhancers, with an odds ratio of 5.12 ($\rho = 2.59 \times 10^{-5}$).

Discussion: Exposure to high concentrations of diuron decreased the viability of MSCs and could therefore affect osteoblastic differentiation and bone mineralization. This pesticide also disrupted osteoclasts maturation by impairing the expression of cell-identity determining genes. Indeed, at sublethal concentrations, differences in the expression of these key genes were mild during the course of *in vitro* osteoclast differentiation. Taken together our results suggest that high exposure levels of diuron could have an effect on bone homeostasis. https://doi.org/10.1289/EHP11690

Introduction

Bone tissue is maintained through continual bone remodeling during the life of an individual. This process involves mainly two cell types: the osteoblasts and the osteoclasts, respectively producing and resorbing the bone matrix. Osteoclasts derive from the hematopoietic lineage through the action of two essential molecules, colony-stimulating factor 1 (CSF-1), and receptor activator of nuclear factor kappa-light-chain-enhancer of activated B cells (NF-κB) ligand (RANKL) expressed by osteoblasts.[1] A tight control of the activities of these two cell types is essential for bone health given that an imbalance seems to be correlated to multiple bone diseases, including osteoporosis,[2] but also characteristic of bone sarcomas.[3]

The tumor necrosis factor (TNF) receptor family RANK, in association with its ligand RANKL, induces the expression of a key osteoclast differentiation transcription factor (TF), nuclear factor of activated T cells, cytoplasmic 1 (NFATC1), through the action of Fos proto-oncogene, AP-1 transcription factor subunit (c-FOS) and TNF receptor-associated factor 6 (TRAF6).[4] This essential step of osteoclastogenesis results in the formation of multinucleated polarized cells that can tightly bind to the bone surface. The resorptive activity of osteoclasts depends highly on their capacity to create an acidic environment on the bone surface. Thus, mutations on the T cell immune regulator 1 gene (*TCIRG1*), encoding for a subunit of the proton secreting ATP6i complex, caused osteopetrosis.[5] Mature osteoclasts also secrete major lytic enzymes: cathepsin-K and tartrate-resistant acid phosphatase (TRAP), encoded by acid phosphatase 5 and tartrate-resistant genes (*CTSK* and *ACP5*), respectively.[6]

Enhancers are *cis*-regulatory DNA elements that play an important role in controlling the expression of cell-type–specific genes.[7] Super-enhancers are chromatin regions characterized by a high acetylation of the histone H3K27, a high methylation of H3K4, as well as an important binding of the mediator and BRD4 proteins.[8,9] As such, they seem to more efficiently recruit the transcriptional complex and induce expression of their target genes compared with typical enhancers.[10] What is more interesting in the study of super-enhancers is their ability to induce expression of master TFs, a subset of TFs that are responsible for defining cell identities.[9] Hence, mapping of super-enhancer targets could be useful to identify key cell-identity driving TFs.

3-(3,4-Dichlorophenyl)-1,1-dimethylurea (diuron) is a phenylurea-class herbicide widely used around the world. Owing to its environmental toxicity and suspected effects on human health, its use is banned or strictly restricted to use on hard surfaces in

*These authors contributed equally to this work.

Address correspondence to Steven Georges, CRCI2NA/UMR1307, 1 Rue Gaston Veil, 44035, Nantes, France. Telephone: (33) 272 641 142. Email: Steven.Georges1@univ-nantes.fr. And, Benjamin Ory, CRCI2NA/UMR1307, 1 Rue Gaston Veil, 44035, Nantes, France. Telephone: (33) 272 641 142. Email: benjamin.ory@univ-nantes.fr

Supplemental Material is available online (https://doi.org/10.1289/EHP11690).

The authors declare no conflict of interest and do not disclose any financial interests in connection with this work.

Received 8 June 2022; Revised 25 April 2023; Accepted 28 April 2023; Published 12 June 2023.

Note to readers with disabilities: *EHP* strives to ensure that all journal content is accessible to all readers. However, some figures and Supplemental Material published in *EHP* articles may not conform to 508 standards due to the complexity of the information being presented. If you need assistance accessing journal content, please contact ehpsubmissions@niehs.nih.gov. Our staff will work with you to assess and meet your accessibility needs within 3 working days.

many countries, such as in France.[11] Despite regulations, diuron is one of the most detected herbicides in our environment, particularly in water.[12–14]

The European Chemicals Agency (ECHA) classified diuron as very toxic to aquatic life with long-lasting effects and as suspected of causing cancer.[15] Moreover, the U.S. Environmental Protection Agency listed it as a likely human carcinogen in 1997.[16]

Reports have claimed that diuron and its residues affect fertilization and embryo development of invertebrate aquatic species,[17] cause hormonal disturbance in fish,[18,19] and are toxic to prokaryotic algae and cyanobacteria.[17] Furthermore, diuron is suspected to be harmful to mammal health. It has been shown to be cytotoxic *in vitro* in human cells, partially through oxidative stress.[20] A carcinogenic potential of diuron exposure is also suspected by *in vitro* and *in vivo* studies. Diuron at high dietary levels in the rat (110 mg/kg for male and 200 mg/kg for female) induced bladder hyperplasia after 20 wk of exposure and neoplasia after 2 y according to a 2002 study from the California Office of Environmental Health Hazard Assessment (OEHHA).[21] Recently Briand et al. showed, in a xenograft mouse model, that diuron alone was not oncogenic in glioma, but that it could participate in tumorigenesis when it was associated with other events, such as overexpression of Akt.[22] Moreover, an *in vivo* experiment on rats showed a large spectrum of effects of diuron, including damage to red blood cells resulting in anemia, liver effects, or splenotoxicity.[23] Despite many *in vivo* studies, the impact of diuron on bones is largely unknown, even though few data suggest a disturbance in bone development. When pregnant rats were exposed to high concentrations of diuron, some offspring showed abnormal bone growth, namely a delayed ossification of the calvarium.[24]

The aim of our study was to better characterize differentiation and maturation of $CD14^+$ monocytes into osteoclasts and to evaluate the impact of diuron exposure on bone homeostasis, particularly in osteoblastic and osteoclastic differentiations. To this end, we first identified genes that are key for osteoclastogenesis by predicting target genes of pro-differentiation super-enhancers. Mapping target genes of super-enhancers that were differentially activated during osteoclastogenesis allowed us to make a comprehensive list of key genes in osteoclast differentiation. Then, the effect of diuron on these genes was evaluated to gain a deeper insight into the impact of diuron exposure on osteoclastogenesis.

Material and Methods

Diuron Preparation

Diuron from Santa Cruz [Chemical Abstracts Service (CAS) 330-54-1, sc-239818; Santa Cruz Biotechnology] was used for all *in vitro* studies. It was dissolved in dimethyl sulfoxide (DMSO; Sigma-Aldrich) at 100 mM, stored at 4°C and added in the cell culture medium at the required concentration, as noted. DMSO was used as the control (corresponding to the percentage of DMSO with the high concentration of diuron, i.e., between 0.01% and 0.1%, according to the experiments).

Osteoblasts Differentiation and Mineralization

At day 0, human mesenchymal stem cells (hMSCs) from two different healthy donors (patients #1 and #2) were seeded at 10,000 cells/well in 48-well plates in minimum essential medium alpha 1X (alphaMEM; 22571-020; Thermo Fisher Scientific) supplemented with 5% platelet lysate and plasma (PLP), heparin (1 UI/mL; Panpharma) and 1% penicillin/streptomycin (09-757F; Lonza). hMSCs and PLP were provided by the Institute for Clinical Transfusion Medicine and Immunogenetics Ulm (IKT Ulm). Briefly, hMSCs were isolated following the single-step protocol developed by the Ulm's institute for transfusion.[25,26] Complete medium (CMSSP) consisted of alphaMEM (Lonza), supplemented with 10% platelet lysate (IKT Ulm), and 2 IU sodium-heparin/mL complete medium. Unprocessed bone marrow was seeded in a first step at a density of 12,000 mononuclear cells (MNCs)/cm^2 on 5-chamber CellStacks (Corning) in 750 mL of CMSSP. After 3 d, the supernatant containing the nonadherent cells was removed, the cells were rinsed with phosphate-buffered saline (PBS) without calcium or magnesium cations (Lonza), and 700 mL of CMSSP was added. The partial exchange of 300 mL of CMSSP was performed twice weekly. After 10–14 d, the cells were rinsed with PBS and harvested using TRYPZEAN (Lonza). After 3 d of expansion, freshly prepared ascorbic acid (50 μg/mL, A-4034; Sigma-Aldrich), β-glycerophosphate (10 mM, G9422; Sigma-Aldrich), and dexamethasone (10^{-7}M; D4902; Sigma-Aldrich) were added into the culture medium to allow mineralization, either in the presence of DMSO (0.1% corresponding to the highest concentration of DMSO used with diuron) or different concentrations of diuron, ranging from 0.78 to 100 μM (obtained by serial dilution). The osteogenic medium was changed twice a week. Alizarin red staining was used to detect the mineralized nodules formed *in vitro*. Between days 13 and 14 and after PBS washing, the cells were fixed in ice-cold 70% ethanol for 1 h and incubated with alizarin red (40 mM, pH 7.4; TMS-008; Sigma-Aldrich) for 10 min at room temperature (RT). After extensive washing with molecular biology-quality water (Eurobio), images were captured with an Axiocam 105 color camera (Zeiss) fitted to a Stemi 2000-C microscope (Zeiss). Mineralized surfaces were quantified using the Image Pro-Plus software (version 6.0; Media Cybernetics). Information about all donors are available in Excel Table S1.

Isolation of $CD14^+$ Premonocytes

The generation of osteoclasts from human $CD14^+$ premonocytes was described previously.[27] Briefly, peripheral blood mononuclear cells were purified from healthy donors using a Ficoll gradient (centrifugation 20 min, 2,000 rpm, at RT), and magnetic-activated cell sorting was used (LS Columns, 130-042-401, and CD14 microbeads human, 130-050-201; Milteny Biotec) to isolate $CD14^+$ cells. Except for the Ficoll step, each centrifugation lasted 10 min at 1,800 rpm. Every protocol step was performed at RT. Information relative to experimental reproducibility and donors used in the different experiments are listed in Excel Table S1. The seven donors consisted of six men and one woman, ranging from 39 to 64 years of age (mean = 53.29 y).

Osteoclast Differentiation

$CD14^+$ cells from three healthy donors (patients #3, #6, and #7) were seeded at 45,000 cells/well in 96-well plates in alphaMEM with 10% fetal bovine serum (FBS; S1810-500; Biowest) and 25 ng/mL human macrophage colony-stimulating factor (MCSF; 216-MC-0025; R&D systems) with 6 wells/condition. After 3 d of expansion, 100 ng/mL hRANKL (donated by Amgen Inc.) was added in the presence of either DMSO (0.025% corresponding to the highest concentration of DMSO used with diuron) or different concentrations of diuron ranging from 0.38 μM to 25 μM (obtained by serial dilution). The osteoclastic medium was changed twice per week. After 7 or 8 d of differentiation, TRAP staining was performed with acid phosphatase, Leukocyte (TRAP) Kit (387A; Sigma-Aldrich) in accordance with the recommendations of the supplier. Images were captured using with an Axiocam 105 color camera (Zeiss) fitted to a Stemi 2000-C microscope (Zeiss). TRAP-stained multinucleated cells formed

with three or more nuclei were counted manually using ImageJ software.[28]

Viability Assay

$CD14^+$ monocytes (from four donors, patients #3, #4, #5, and #6) or MSCs (from three donors, patients #1, #2, and #3) were plated in 96-well plates at 45,000 and 3,500 cells/well, respectively, and then treated with DMSO (0.025% and 0.1%, respectively, corresponding to the highest concentration of DMSO used with diuron) or different concentrations of diuron as noted (respectively, 0.38–25 μM and 0.78–100 μM). Six wells per condition were performed. After 7 d of treatment, the cells were fixed with 1% glutaraldehyde (G62557; Sigma-Aldrich) under agitation for 5 min, washed with water, and then stained with 0.1% crystal violet (HT901-8F02; Sigma-Aldrich) for 5 min. After drying, the dye was diluted 5 min in Sorensen's buffer (trisodium citrate, hydrochloric acid 0.1N, and ethanol; Sigma-Aldrich) and the absorbance was measured at 570 nm using a spectrophotometer (1420 $Victor^2$; Perkin Elmer). The proliferation rate is represented as a percentage of cells treated with DMSO only.

Quantitative Reverse Transcription–Polymerase Chain Reaction

After osteoclastic differentiation of $CD14^+$ cells (from four donors, patients #3, #4, #6, and #7) seeded at 1.2 million cells/well in 6 wells in the presence of DMSO (0.01%) or different concentrations of diuron (0.1 μM, 1 μM, or 10 μM), total RNA was extracted from cultured cells at day 7 or day 10 using the Nucleospin RNA Plus kit (740984.250; Macherey-Nagel) according to the protocol of the manufacturer. Total RNA was reversed transcribed using the Maxima H Minus First Strand cDNA Synthesis Kit (K1652; Thermo Fisher Scientific). Real-time monitoring of polymerase chain reaction (PCR) amplification of complementary DNA (cDNA) was performed in duplicate using validated DNA primers (Eurogentec) on CFX96 real-time PCR detection system (Bio-Rad) with SYBR Select Master Mix (4472908; Applied Biosystems) following the PCR program shown in Excel Table S2. Primer sequences are available in Excel Table S3. Target gene expressions were normalized to glyceraldehyde 3-phosphate dehydrogenase (GAPDH) levels in respective samples as an internal standard, and the comparative cycle threshold (Ct) method was used to calculate relative quantification of target mRNAs. Experiments were performed once per donor, except for donor #3 for whom the experiment was carried out twice.

H3K27ac ChIP-Sequencing

A total of 1.2 million $CD14^+$ monocytes/well from two healthy donors (patients #1 and #2) were seeded in a 6-well plate and differentiated into osteoclasts as described above. After 3 d of proliferation (without differentiation medium) and at day 7 and at day 10 of culturing with or without differentiation medium, cells were washed twice with PBS and then treated 10 min at 37°C with accutase solution (A1110501; Gibco) to gently remove cells. The experiment was done in duplicate for each donor. Cells from six wells were pooled and centrifuged for 15 min at $400 \times g$ and resuspended with PBS. Pellets were suspended with a 1% formaldehyde-PBS (28908; Pierce Biotechnology) solution and incubated for 10 min at 37°C to cross-link cells. A 5% glycine solution (50046; Sigma-Aldrich) was added to stop cross linking, and the samples were incubated for 5 min at 37°C. The cells were spun down at $320 \times g$ for 5 min, and the pellets were resuspended with PBS containing protease inhibitors (11873580001; Roche). This step was repeated twice, and the pellets were then flash frozen in liquid nitrogen. Samples were stored at −80°C and sent to ChIP-sequencing (ChIP-Seq) platforms at the Broad Institute (Boston, MA, USA). To identify super-enhancers, ChIP-Seq was performed using H3K27ac antibodies [acetyl-histone H3 K27 (D5E4) XR Rabbit mAB; 8173P; Cell Signaling Technologies] at the Broad Institute's Genomics Services platform. Libraries preparations and sequencing were performed in a multiplexed system for 96 samples as reported earlier.[29] Input libraries preparations and sequencing were done at Active Motif Inc (Carlsbad, CA, USA). Prepared libraries were sequenced using Illumina's HiSeq2500 in 2×100 bp format for the ChIP data and using Illumina's NextSeq500 in a 1×75 bp format for the input data.

RNA-Sequencing

For the differentiation data set, RNA-sequencing (RNA-Seq) was performed in triplicate for $CD14^+$ monocytes from patient #2 at day 3 without differentiation medium, at day 7 with or without differentiation medium, and at day 10 with or without differentiation medium at Active Motif Inc. For the diuron effect data set, cells were treated with either DMSO (0.01%) or diuron (10 μM) plus the differentiation medium. Cells were harvested at day 3 and at day 10 for RNA-Seq. The Illumina's TruSeq Stranded mRNA Sample Preparation Kit was used for libraries preparation, and sequencing was done using Illumina's NextSeq 500 in 2×42 bp mode.

Data Treatment

ChIP-Seq. Read mapping was performed using bwa mem (version 0.7.17)[30] against the human genome hg19. Low-quality reads (-q 20) and PCR duplicates were removed from bam files using samtools (version 1.9). To remove technical replicate specific signals, bam files of technical replicates were merged. Peak calling was then performed using MACS2[31] with recommendations given on MACS2's Git Hub page. The peak calling pipeline consists of generating coverage tracks for the ChIP and input data separately. This pipeline can be found as a snakemake file on the lab's GitHub page (https://github.com/EpistressLab).

1. We first filtered duplicate reads from both ChIP and input data using macs2 filterdup, keeping only one read.
2. Fragment lengths were then estimated for the ChIP data using a script (sam_insert-size.pl) from the bac-genomics-scripts by sampling 2 million reads from the ChIP sample.[32] Macs2 predictd was used to estimate fragment length for the input sample.
3. ChIP sample coverage track was then built by extending reads to meet fragment length.
4. Multiple coverage tracks were then generated for the input sample using macs2 pileup. Input reads were extended in both directions with half of the estimated fragment length (d background), with 500 bp (1 kb slocal background) and with 5,000 bp (10 kb llocal background). The genome background was then calculated by multiplying the total number of reads in the input sample by the ratio of fragment length and genome size (2.7×10^9). The slocal and llocal coverages were corrected by multiplying them with the ratios of ChIP fragment lengths, to 1,000 and 10,000, respectively (macs2 bdgopt). The maximum of these different corrected input coverages (d background, slocal, llocal, and genome backgrounds) was then computed for each genomic location (macs2 bdgcmp). The maximum biases for each genomic location formed the local bias bedgraph file.
5. The ChIP and input samples were scaled to the same sequencing depth. For this the local bias bedgraph file was multiplied by the ratio of total number of reads in the ChIP

sample by the total number of reads in the input sample using macs2 bdgopt.

6. Then ChIP and input coverages were compared using macs2 bdgcmp to produce the scores in q-values through a local Poisson test.
7. Peaks were then called using macs2 bdgpeakcall with a q-value threshold for peak significance set at 1×10^{-5}.

RNA-Seq. Fastp[33] (version 0.19.5) was used to filter low-quality reads ($Q < 30$) and to trim remaining PCR adapter sequences. Filtered reads were mapped to the human genome hg19 using HISAT2[34] (version 2.1.0), then read quantification on gene and transcript level was performed using stringtie[35] (version 2.1.1). Gencode's GRCh37 (version 35) was used for gene annotation. R package DESeq2[36] was then used to normalize and extract significantly differentially expressed genes between different conditions. The same sequencing protocol and data analysis pipeline were used for the diuron-treated samples. To identify differentially expressed genes during differentiation within cells treated with either DMSO or diuron in a full model, that is, considering time and treatment, the likelihood-ratio test (LRT) was used with an adjusted p-value threshold of 0.05. For pairwise comparisons, the Wald test was performed and $\log_2$-fold-changes were shrunken. Genes were identified as significantly differentially expressed if the absolute value of their $\log_2$-fold-change was >1 and the adjusted p-value was <0.05. Gene set enrichment analysis (GSEA) and overrepresentation analysis (ORA) were performed using the R package ClusterProfiler.[37] For GSEA, genes were preranked using shrunken $\log_2$-fold-changes (DESeq2's lfcShrink function), and enrichment was performed against gene sets from either Reactome.db[38] or Gene Onotology's Biological Processes (GO:BP). For overenrichment analysis, differentially regulated genes were selected using the aforementioned thresholds for adjusted p-values and $\log_2$-fold-changes, then enrichment for gene sets was performed against Reactome.db or GO:BP. For both analyzes, a p-value threshold of 0.05 was used to select significantly enriched or overrepresented gene sets. Among the significantly enriched gene sets, only those involved in osteoclastogenesis or bone remodeling are represented in the figures, for the sake of readability more details on these analyzes can be found in the scripts publicly available on our GitHub page (https://github.com/EpistressLab/OC_diuron_paper).

To validate our differentiation model, we established a list of 40 genes that are of interest in osteoclastogenesis based on the literature (Excel Table S4). We hereafter refer to this list as genes of interest in this article. The names and the expression levels of the genes included in this list can be found in Figure 1E. The expression levels in the figure were normalized using DESeq2's median of ratios method (see DESeq2's user's manual[39] for more details if needed).

Heatmaps of significantly differentially expressed features represent row z-scores. The z-scores were calculated on normalized log-transformed counts (DESeq2's rlogTransformation function). For each feature (gene or regulatory DNA element) in a row, values were subtracted from the average feature count across all samples and divided by the standard deviation (SD) of the feature across all the samples (R base's scale function). As such, the per-row average is brought to 0 and the SD to 1. This allows the capture of feature variability across samples and its representation in a color-coded, easy-to-read manner. For the sake of transparency, the z-score values underlying the heatmaps are provided as supplementary material (Excel Tables S5, S11, S25, S26, S29).

Super-enhancers identification and target genes prediction. To identify super-enhancer regions, the ROSE2 algorithm was used.[9,40] Super-enhancers identified in the different samples were gathered and read counts were quantified using Rsubreads's featureCounts function.[41] For this, the allowMultiOverlap argument was set to True, to include reads within overlapping regions, and requireBothEndsMapped was set to True, to ignore single-end reads. Then overlapping regions were filtered using chromVAR's filterPeaks function, keeping the regions with the highest read counts. Normalization of read counts was then processed using EDASeq[42] and a script from Ott et al., based on biases in read counts within regions of equivalent GC content.[43] Normalization factors calculated as such and raw read counts were added in a DESeq2 object. The same procedure was performed to analyze identified typical enhancers. To have a consistent normalization process, bigWig tracks for data visualization were normalized using normalization factors from the DESeq2 object of all enhancers data. For this, normalized bigWig tracks coverage files were generated using deeptools' bamCoverage[44] with -scaleFactor argument taking the median of normalization factors for the corresponding sample in the DESeq2 object. To check the quality of the normalization process, normalized counts were extracted at the promoters of known housekeeping genes that we expected to be unchanged (Figure S1). To functionally annotate super-enhancers, that is, to assign them a target gene, genes within the topologically associated domains [TADs, as defined in human embryonic stem cells (ESCs) by Dixon et al.[45]] of each super-enhancer were identified. TADs correspond to genomic regions that display higher frequency of contacts inside the TAD than outside the TAD and a strong conservation across cell types and even across mammalian genomes.[45–48] These domains were revealed using HiC, a genome-wide chromatin interactions mapping technique first described in 2009.[49] Given that regions within the same TAD have higher frequency of contact between them, enhancers and target genes are suggested to be found within the same TAD.[50] Hence, among the genes found within the TAD of the super-enhancer considered, those showing fold-differences in the same direction as the super-enhancer were kept. With this approach, a gene was considered a target of a super-enhancer if and only if the gene was found within the same TAD as the super-enhancer and if the gene was significantly differentially expressed in a manner where the fold-differences of the super-enhancer and the gene were in the same direction.

Statistical analysis for Table 1. To test whether target genes of super-enhancers activated or gained during *in vitro* osteoclastic differentiation are significantly affected when cells are exposed to diuron, the list of predicted target genes of gained super-enhancers were compared with the list of genes affected by exposure to diuron (for genes significantly differentially expressed according to the LRT with adjusted $p < 0.05$ considering both time and treatment effect; Figures 2A and 4A; Figure S7). For the Fisher's exact test, the background was considered to be all genes that were detected (normalized counts >20) in at least one of the samples in our RNA-Seq data. This is because one of the criteria to consider genes as targets of super-enhancers is if they are differentially expressed, and for this they need to be detected in at least one of the samples. Among the genes annotated by Gencode (GRCh37; version 35), all those detected in our RNA-Seq were considered as background (Table 1 presents the sizes of the lists).

Motif analysis. For the motif enrichment analysis we chose to work on the differentially activated enhancers and not the super-enhancers, given that the number of differentially activated super-enhancers was low. By considering all the enhancers, we could obtain a more comprehensive overview of the effector transcription factors that could be recruited in the regulatory DNA elements. After identifying gained and lost enhancers at day 7 and at day 10 with differentiation medium compared with day 3 without differentiation medium (Wald test, $|\log-_2\text{fold-change}| > 0.7$ and adjusted $p < 0.1$), potential actors in the differential enhancers were predicted by looking for known TF binding sites. For this, memesuite's Analysis of Motif Enrichment (version 5.3.3; AME) was used to perform differential enrichment between sequences of gained and lost enhancers at day 7, for example.[51] As such, four

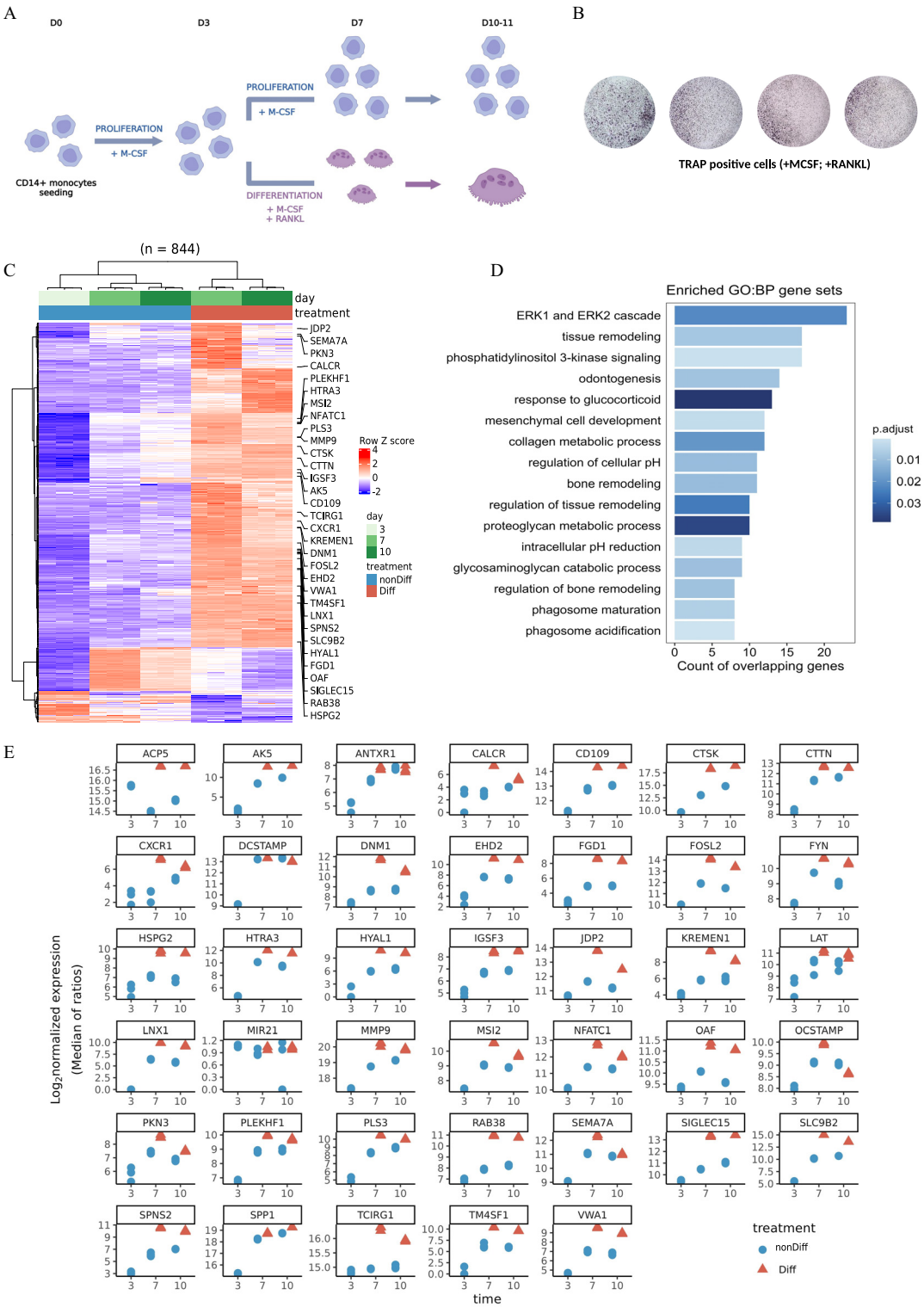

Figure 1. Functional and transcriptional characterization of the applied *in vitro* osteoclast differentiation model. (A) schematic representation of the osteoclast differentiation protocol. $CD14^+$ premonocytes were treated with either differentiation medium or left with the proliferation medium for 4 d (day 7) or 7 d (day 10). TRAP staining was then performed on day 10. Cells were also harvested at day 3 (initial day of differentiation), day 7, and day 10 for RNA-Seq. (B) Images of TRAP staining at day 10 of differentiation of $CD14^+$ monocytes (medium complemented with MCSF and RANKL) from four different donors [patients #3, #4, #6, and #7 (Excel Table S1)] into osteoclasts (magnification 40×). (C) Relative expressions of significantly differentially expressed genes in subsequent pairwise comparisons of (day 7+ diff vs. day 7 − diff) and (day 7+ diff vs. day 3 − diff) (Wald test, $|\log_2\text{-fold-change}| > 1$, $p < 0.05$; Excel Tables S6 and S7 provide outputs of the two comparisons, Excel Table S5 provides *z*-scores underlying the heatmap). (D) Overrepresented GO:BP terms in the list of genes from C. (E) Log_2-normalized abundances of selected genes (list in Excel Table S4) at different time points and culture conditions (individual values in Excel Table S8). Note: D, day; Diff, differentiation; GO:BP, Gene Onotology's Biological Processes; MCSF/M-CSF, macrophage colony-stimulating factor; nonDiff, non-differentiation; p.adjust, adjusted *p*-value; RANKL, nuclear factor kappa-light-chain-enhancer of activated B cells ligand; RNA-Seq, RNA sequencing; TRAP, tartrate-resistant acid phosphatase.

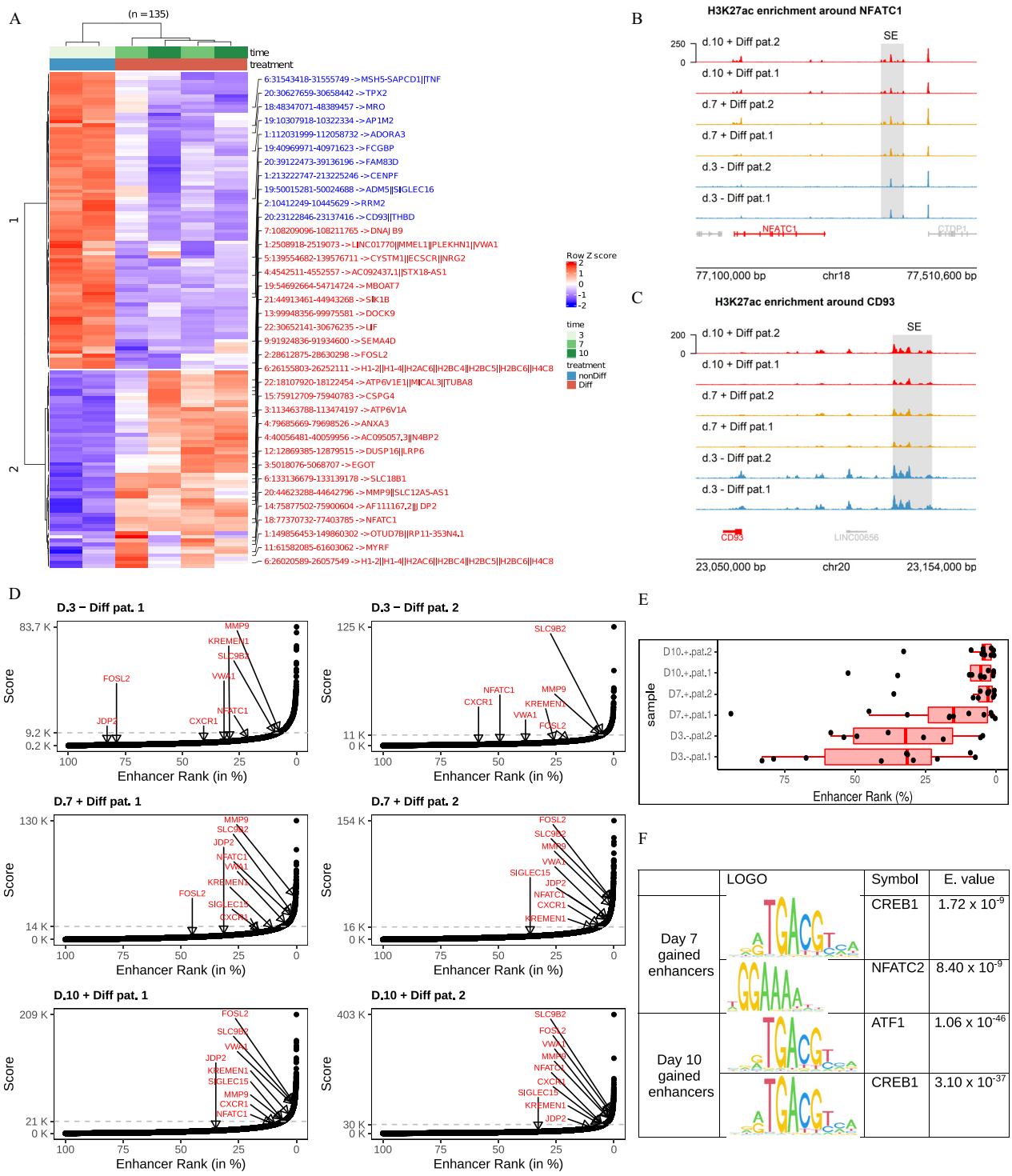

Figure 2. Transcriptional modifications and super-enhancer mapping during osteoclast differentiation. CD14$^+$ premonocytes from two donors [patients #1 and #2 (Excel Table S1)] were treated with differentiation medium for 4 d (day 7) and 7 d (day 10), then cells were harvested at day 3 (initial day of differentiation), day 7, and day 10 for anti-H3K27ac ChIP-sequencing. (A) Relative H3K27ac read counts within significantly differentially active super-enhancers (annotated with their potential target genes) in the comparison day 7 with differentiation medium vs. day 3 without differentiation medium (z-score values underlying the heatmap are provided in Excel Table S11, and Wald test output is provided in Excel Table S12). (B) H3K27ac signal coverage plot from normalized bigWig files (see the "Material and Methods" section for the normalization process) around *NFATC1* region; (C) *CD93* region; (D) hockey stick plot representing H3K27ac signal vs. enhancer rank in percentile × 100 (can be read as the percentage of enhancers with higher score values). (E) Box plot showing rank positions of regulatory regions (enhancers/super-enhancers) overlapping super-enhancers predicted to induce genes of interest (midline: average; box limits: 1st and 3rd quartiles; whiskers: 5th and 95th quantiles; see Excel Table S28 for statistical summary). (F) Differential motif enrichment within sequences of gained enhancers at day 7 or day 10 compared with enhancers specific to day 3 (lost enhancers) was performed using meme-suite's analysis of motif enrichment (AME). Sequences of gained enhancers were used as primary sequences and those of lost enhancers as control/background sequences. Figure presents top significantly differentially enriched motifs (AME analysis summary with E. value corresponding to the expected number of random motifs that would be as enriched as the considered motif in the primary sequences. E. value is calculated as the adjusted p-value multiplied by the number of motifs in the motif database; see AME's user's manual for more detail; https://meme-suite.org/meme/doc/ame.html). Note: ChIP, chromatin immunoprecipitation; chr, chromosome; Diff, differentiation; E. value, expected value; pat, pattern; nonDiff, non-differentiation; SE, standard error.

Table 1. Summary of Fisher's exact test result when comparing overlap between the lists of diuron-affected genes and genes targeted by gained super-enhancers during osteoclastic differentiation at day 10.

	Diuron-affected			
	In-house association		High-confidence association	
	Yes	No	Yes	No
Gained super-enhancers targets (day 10)				
Yes	11	111	10	45
No	424	21,916	425	21,982
Fisher's exact test	OR = 5.12 (95% CI: 2.74, 9.58) $p = 2.59 \times 10^{-5}$		OR = 11.49 (95% CI: 5.13, 23.31) $p = 8.99 \times 10^{-8}$	

Note: Diuron-affected genes are identified thanks to the LRT test considering both time and treatment (Figure 4A; Excel Table S25). Target genes of gained super-enhancers correspond to genes associated to super-enhancers that gain H3K27ac signal at day 10 in differentiation medium–treated cells (Excel Table S13: $\log_2$-fold-changes >0; columns: "target" for in-house association and "target_symbols" for high-confidence association). In the 3rd and 4th columns are presented numbers from our super-enhancer-gene associations, and in the 5th and 6th columns are presented numbers from the high-confidence list of associations cross-validated with PEGASUS (Predicting Enhancer Gene Associations Using Synteny). CI, confidence interval; LRT, likelihood-ratio test; OR, odds ratio.

analyses were performed by using sequences in gained enhancers day 7 vs. sequences in lost enhancers day 7, and then lost enhancers day 7 vs. gained enhancers day 7, and likewise for day 10.

Results

Validating the in Vitro *Differentiation Protocol by Tracking Transcriptional Modifications Occurring during OC Differentiation*

In an effort to first validate our differentiation protocol, we sought to characterize the transcriptional modifications occurring during osteoclast differentiation under normal conditions. After a 3-d long proliferative phase, involving culturing purified $CD14^+$ monocytes with MCSF, the culture medium was complemented or not with RANKL (Figure 1A). To validate formation of mature osteoclasts, we first performed TRAP staining at day 10 of the differentiation protocol, and we visually assessed the $TRAP^+$ cells (Figure 1B). RNA-Seq on $CD14^+$ cells treated with or without differentiation medium for either 4 (day 7) or 7 (day 10) d was performed. For each time point (day 7 and day 10), pairwise comparisons were made between differentiation medium–treated ($mCSF^+$; $RANKL^+$) and proliferation medium–treated ($mCSF^+$; $RANKL^-$) cells (Figure 1C), as well as between differentiation medium–treated cells (at day 7 or day 10) and day 3 proliferation medium–treated cells to identify genes differentially expressed owing to the differentiation medium. Genes that were significantly differentially expressed (adjusted $p < 0.05$ and $|\log_2 FC| > 1$) in both comparisons were extracted (Figure 1C; Excel Tables S5–S7) and an ORA analysis for each time point was performed against GO:BP gene sets. Starting from day 7, "bone remodeling" and "glycosaminoglycan catabolic process" were among the top significantly overrepresented gene sets, as expected (Figure 1C,D). At day 10, an overrepresentation of "glycosaminoglycan catabolic process" and "collagen metabolic process" was observed (Figure S2A,B). A list of genes that participate in osteoclast differentiation or activity was established based on the literature and our experience (see Excel Table S4 for references), to validate our differentiation model. Plots of the expression of individual genes of interest demonstrated the evolution of expression of these genes during the osteoclastic differentiation process (Figure 1E; Excel Table S8). An early increase in mRNA levels of osteoclast stimulatory transmembrane protein (*OCSTAMP*), *ACP5*, *CTSK*, *NFATC1*, matrix metallopeptidase 9 (*MMP9*), and *JDP2* can be mentioned.

Transcriptional Modifications and Super-Enhancer Mapping during Osteoclast Differentiation

The epigenetic landscape was then tracked to understand the onset of the transcriptional program during the osteoclastic differentiation process. ChIP-Seq using antibody targeting H3K27ac was performed on $CD14^+$ cells treated with differentiation medium for either 7 or 10 d and on $CD14^+$ cells harvested after the proliferation phase and before treatment with differentiation medium (day 3 proliferation medium–treated cells). As described earlier, H3K27ac is a marker of transcriptionally active promoters and active enhancers.[52,53]

Analysis was started by looking into enhancers. Differentially active enhancers between differentiation medium–treated cells (d7.+diff and d10.+diff) and proliferation medium–treated cells (d3.– diff) were extracted (adjusted $p < 0.1$ and $|\log_2 FC| > 0.7$). Genes found within the corresponding TADs (as defined by Dixon et al.[45]) of these enhancers were determined and tested if their expressions were also altered during the differentiation process. The purpose of this process was to functionally annotate enhancers by checking for coherence between gene expression and H3K27ac signals in enhancers. Using this approach, we were able to identify 489 and 1,519 enhancers that showed a significantly higher H3K27ac signal in differentiated cells at day 7 and day 10, respectively, compared with day 3 undifferentiated cells (Excel Tables S9 and S10). We will refer to these as gained enhancers going forward. Their potential target genes, required to be within the TADs of these enhancers and to be significantly up-regulated in differentiated cells, were extracted and ORA was performed on these genes. Target genes of gained enhancers at day 7 ($n = 227$) showed significant overrepresentation of "phagosome acidification," "extracellular matrix organization," "monovalent inorganic cation homeostasis" among others, suggesting the support of the transcriptional program by the epigenetic landscape during differentiation (Figure S3A). At day 10 ($n = 644$), overrepresentation of "bone remodeling" and "collagen catabolic process" was observed (Figure S3B). In total, 871 associations were obtained between significantly up-regulated genes and gained enhancers, among which *NFATC1*, *MMP9*, FOS like 2 (*FOSL2*), C-X-C motif chemokine receptor 1 (*CXCR1*), and *CD109* were labeled as targets (Figure 2B,C). As such, we were able to associate 17 of the 40 genes of interest, to be colocalized within the TADs of gained enhancers during $CD14^+$ cells differentiation into osteoclasts.

On the other hand, lost enhancers (enhancers with significantly reduced H3K27ac enrichment during the course of osteoclast differentiation) seemed to regulate genes involved in more diversified biological processes. Innate and adaptive immune signatures seemed, however, to be highly present among the overrepresented gene sets. "Positive regulation of mast cell activation," "cytokine secretion," and "leukocyte migration" could be noted (Figure S3C,D). For the lost enhancers, we were able to assign 648 genes in total. Among these genes, we can mention *CD93* (Figure 2C) and Fc receptor like A (*FCRLA*) (Figure S4G). A

differential motif enrichment analysis was performed using AME from meme-suites in the differentially activated enhancers. The analysis at day 7 showed a higher enrichment of NFATC-like and ATF1/3 motifs within the sequences from gained enhancers compared with the lost enhancers, whereas minor allele frequency (MAF)/MAF BZIP transcription factor B (MAFB) motifs were relatively enriched in the sequences of the lost enhancers (Figures S5 and S6).

The analysis was then restricted to super-enhancers to identify genes that are supported by the most highly activated clusters of enhancers. Lost and gained super-enhancers, at day 7 (Figure 2A; Excel Tables S11 and S12) and at day 10 (Figure S7 and Excel Table S12), during the osteoclast differentiation process were identified and annotated to their potential target genes. As such, super-enhancers potentially targeting *NFATC1*, *FOSL2*, and *JDP2* were identified through this analysis (Figure 1; Figure S4). Interestingly, two distinct super-enhancers seemed to support the expression of *FOSL2* and leukemia inhibitory factor genes (*LIF*) expression (Figure S4). In contrast, some super-enhancers present in the progenitor cells seemed to be lost, among these were *CD93* and *FCRLA* (Figure 2C; Figure S4G). Interestingly, a lost super-enhancer during the osteoclast differentiation process was identified close to the *MAFB* gene, and on the other hand, MAF and MAFB motifs seemed to be relatively enriched within lost enhancers compared with gained enhancers at day 7. The association between this lost super-enhancer and *MAFB* gene was not built using our approach owing to the fact that MAFB gene expression seemed to decrease without differentiation medium and so was not specific to the treatment. As a consequence, it was excluded from the potential target genes (Figure S8).

Rank positions of super-enhancer–regulating genes of the preselected genes of interest were compared between different samples. Regulatory regions targeting genes of interest seemed to rank among the regions with highest H3K27ac signal scores, mainly among the top 5% to 10% of all the identified regions within the differentiated samples (Figure 2D,E). The gain of H3K27ac signal within super-enhancer targeting genes of interest seem to occur as early as day 7.

We sought to identify significantly differentially active regions between differentiation medium–treated and proliferation medium–treated cells at day 7 and day 10. When we performed tests of differential activation between differentiation medium–treated and proliferation medium–treated cells at day 10, we identified no significantly differentially enriched enhancers or super-enhancers (thresholds: $\log_2$-fold-change > 0.7 or < -0.7 and adjusted $p < 0.1$). We found 55 differentially enriched enhancers at day 7 between differentiation medium–treated and proliferation medium–treated cells, but none of these enhancers were super-enhancers (Excel Table S14). Proliferation medium–treated cells at day 3 and at late days (7 and 10) displayed numbers of enhancers and super-enhancers differentially enriched comparable to those obtained in the comparison between differentiation medium–treated cells at late days and day-3 proliferation medium–treated cells (Excel Tables S15–S18). It seemed like the proliferation medium alone allowed the setup of active enhancers and super-enhancer; however, there were strong differences at the RNA-Seq level.

We then sought to support our predicted enhancer/super-enhancer–gene associations using conservation of synteny. This is based on the conservation of the positional linkage between enhancers and their associated genes through evolution. We used the associations between conserved noncoding elements (CNEs) and genes in their surroundings performed by Predicting Enhancer Gene Associations Using Synteny (PEGASUS) to verify this information.[54,55] The rationale on the use of this database was, first, because variants in functional noncoding elements could be deleterious especially in developmental enhancers and, second, because conserved synteny or at least conserved positional proximity between enhancers and promoters across evolution could suggest functional associations. When comparing our enhancers/super-enhancers and PEGASUS's CNEs, we observed that between 55% and 60% of active enhancers in our data set overlapped at least with one CNE, whereas the proportion was $\sim 87\%$ in our active super-enhancers. When looking into our associations, we observed that between 43% and 70% overlapped with PEGASUS's associations (Excel Table S19). Going forward, we will address this list of associations cross-validated with PEGASUS as high confidence.

In Vitro *Evaluation of Diuron Effects during Osteoclast and Osteoblast Differentiation*

In the aim to study the potential impact of diuron on bone homeostasis, its effects on osteoclastic cells *in vitro* were evaluated. Purified human $CD14^+$ monocytes were grown with or without a range of diuron concentrations (Figure 3A). No significant effect on cell viability was noticed even at the highest concentration of diuron, suggesting that this pesticide did not affect survival of osteoclastic precursors (Figure 3B; Excel Table S20). Then, the same range of concentrations was used to test whether this herbicide could impair osteoclastic differentiation. $CD14^+$ monocytes from three different donors were differentiated during 7–8 d into osteoclasts with either DMSO or diuron (Figure 3A). Owing to a large variability in the number of mature osteoclasts obtained after differentiation of $CD14^+$ monocytes, data were normalized to 100 for DMSO condition. Interestingly, the cells treated with diuron exhibited impaired osteoclastogenesis, and this occurred in a concentration-dependent manner. The number of osteoclasts per well was lower by 26.5% at 0.38 μM to 88.3% at 25 μM of diuron in differentiation medium (Figure 3C,D; Excel Table S21). Moreover, this inhibitory effect of diuron was associated with a lower gene expression of osteoclastic differentiation markers (Figure 3E; Excel Table S22).

At day 7, the mRNA level of *NFATC1*, a master transcription regulator of osteoclastic differentiation was lower by 75.5% in the presence of 10 μM diuron. No significant differences in expression were noticed at lower concentrations of diuron compared with control. Expression of other osteoclastic markers was not significantly different at day 7 compared with control even though lower expression of cathepsin K (CTSK), a protease expressed predominantly by osteoclasts, and *MMP9*, another protease involved in osteoclastic activity, were observed. At day 10, mRNA levels of *NFATC1*, *CTSK*, and *MMP9* were significantly lower by 69%, 77.8%, and 54.9%, respectively, with 10 μM diuron. Surprisingly, the expression of TRAP was not significantly different from control.

The effect of diuron was also evaluated on osteoblasts, major actors in bone homeostasis. Human MSCs from healthy donors were treated with a large scale of diuron concentrations at day 3 and then cultured for 14 d with proliferation medium (Figure S9A). Osteoblastic precursors exposed to 25 μM diuron and higher concentrations exhibited lower viability than control cells (Figure S9B and Excel Table S23). After differentiation of MSCs from two different donors into osteoblasts in the presence of DMSO or diuron, quantification of calcium deposits through alizarin red staining showed less mineralization starting at 25 μM for donor #1 and at 100 μM for donor #2 in the diuron-treated cells (Figure S9C and Excel Table S24). Because the inhibitory effect of diuron on osteoblastic differentiation could not be distinguished from its impact on

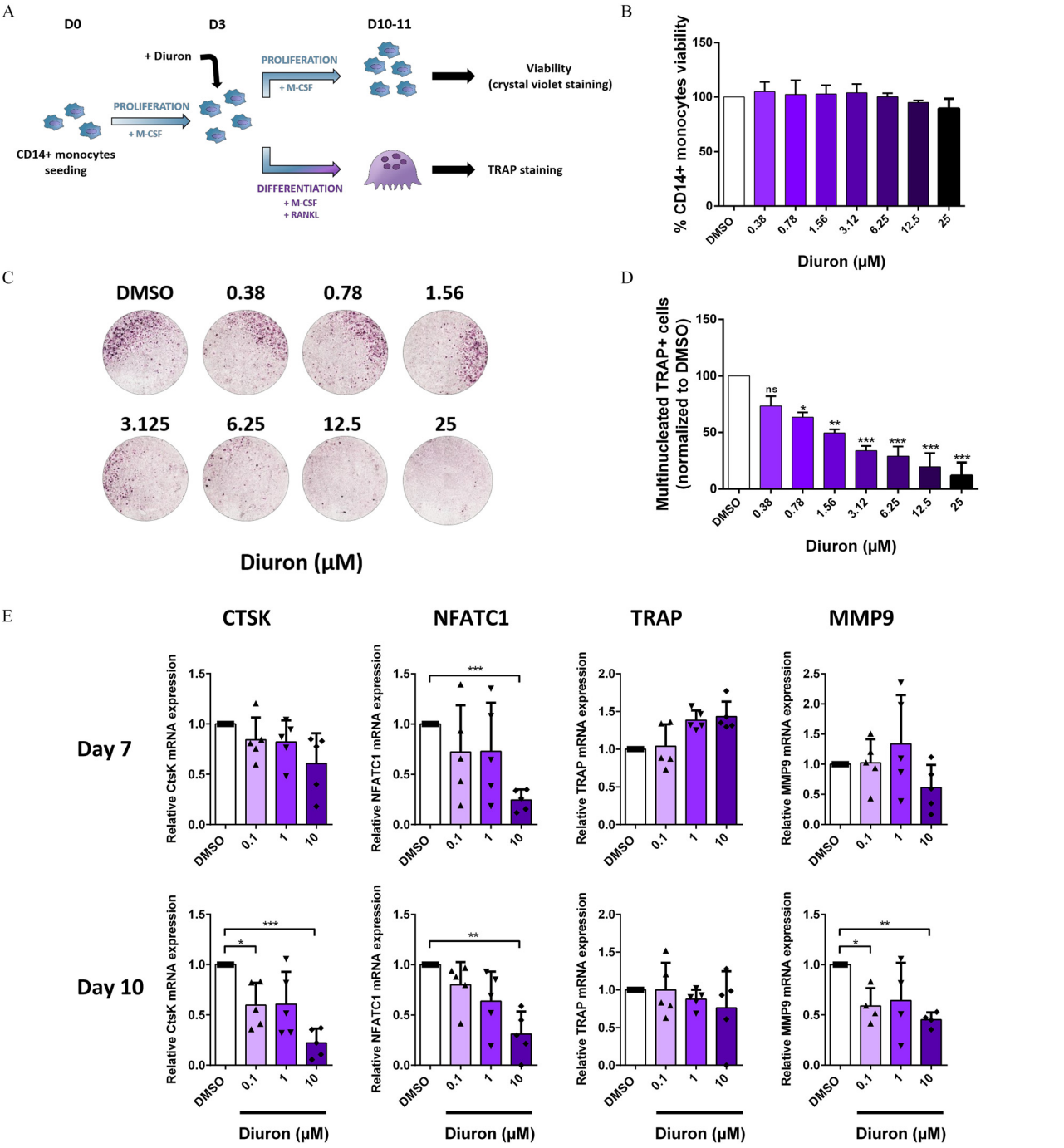

Figure 3. *In vitro* evaluation of diuron effects during osteoclast differentiation. (A) Schematic representation of experimental protocol. Purified human $CD14^+$ monocytes were cultured for 3 d in the proliferation medium (MCSF). DMSO (0.025%) or range of diuron concentrations was added at day 3 and osteoclastic precursors were either maintained in proliferative medium for 7 d to perform crystal violet staining (viability) or cultured with differentiation medium (mCSF + RANKL) for 7–8 d to realize TRAP staining. (B) Cell viability was assessed by crystal violet staining. Results are expressed in percentage of the control condition with DMSO (0.025%) and represent mean ± SD of four independent experiments with $CD14^+$ monocytes isolated from four different donors (patients #3, #4, #5, and #6). Summary data are available in Excel Table S20. (C) Images of TRAP staining at day 10 of differentiation of $CD14^+$ monocytes in 96-well plates in the absence (DMSO 0.025%) or presence of a range of diuron concentrations (magnification 40 ×). TRAP coloration was performed at the end of the culture period. (D) $CD14^+$ purified from three different donors [patients #3, #6, and #7 (Excel Table S1)] were differentiated in the absence (DMSO 0.025%) or presence of a range of diuron concentrations. TRAP coloration was performed at the end of the culture period and multinucleated $TRAP^+$ cells were counted under a light microscope. Data for the cells of each donor are normalized to vehicle control (100%). The graph represents the mean ± SD of three independent experiments, $^{*}p < 0.05$, $^{**}p < 0.01$, $^{***}p < 0.001$, compared with control by one-way ANOVA followed by Dunnett's multiple comparisons test. Summary data are available in Excel Table S21. (E) Purified human $CD14^+$ monocytes from a minimum of four different donors (patients #3, #4, #6, and #7) were cultured for 7 d in the presence of MCSF, RANKL, and three different concentrations of diuron as indicated. DMSO (0.01%) was used as control. mRNA levels of *TRAP*, *cathepsin K*, *NFATc1,* and *MMP9* were assessed by qRT-PCR at the end of the culture period. Data are expressed as fold-change compared with control and represent mean ± SD of five independent experiments, $^{*}p < 0.05$, $^{**}p < 0.01$, $^{***}p < 0.001$, compared with control by one-way ANOVA followed by Dunnett's multiple comparisons test. Summary data are available in Excel Table S22. Note: ANOVA, analysis of variance; D, day; DMSO, dimethyl sulfoxide; MCSF/M-CSF/mCSF, macrophage colony-stimulating factor; RANKL, nuclear factor kappa-light-chain-enhancer of activated B cells ligand; qRT-PCR, quantitative real-time polymerase chain reaction; SD, standard deviation; TRAP, tartrate-resistant acid phosphatase.

osteoblastic precursor viability, we focused our study on the effects on osteoclastogenesis.

Osteoclast Differentiation Transcriptional Profile during 10 μM Diuron Exposure

To study the transcriptomic effect of diuron on osteoclast differentiation, RNA-Seq was performed on $CD14^+$ cells treated with either DMSO or diuron complemented with osteoclast differentiation medium. Cells treated with DMSO or diuron were harvested at day 3 and at day 10. With the intent to evaluate the effect of diuron treatment on the differentiation process, LRT was used to identify differentially expressed genes. The DESeq2 object was assigned a reduced design model that would consider only the individual effects of time and treatment (time + treatment), whereas the full design model included the combination of time and treatment variables (time + treatment + time:treatment). Genes were considered to be significantly differentially expressed if the adjusted p-value was <0.05.

Using this approach, genes that were significantly differentially expressed owing to diuron treatment during the differentiation process were identified. Among these, some were key genes for osteoclast development or function, such as *MMP9,*[56,57] *OCSTAMP,*[58] *TCIRG1,*[5] or *NFATC1*[59] (Figure 4A; Excel Table S25). ORA using GO:BP showed a significant overrepresentation of gene sets linked with osteoclast activity, such as "collagen catabolic process," "extracellular matrix disassembly," and the osteoclast differentiation-driving "calcineurin-NFAT signaling cascade" (Figure 4B). Expression of the 40 genes of interest in the preselected list were tracked in the different conditions (Excel Table S3). To do so, the R package DEGReport,[60] which can classify the differentially expressed genes in different clusters based on the dynamics of their expressions in the different conditions, was used (Figure 4C). The genes of interest were either in the cluster "1" or "5," which are clusters that contain genes expressed higher in the DMSO-treated cells at day 10 but whose difference in expression is significantly lower in the diuron-treated cells.

To check whether the differentiation process occurred properly in the DMSO-treated cells, pairwise comparison using the Wald test was performed between day-10 DMSO-treated and day-3 DMSO-treated cells. GSEA was run against Reactome.db's (Reactome pathway database; https://reactome.org/) gene sets using the significantly differentially expressed genes in this comparison (adjusted p-value threshold <0.05, and $|\log_2 \mathrm{FC}| > 1$). These results, summarized in Figure 4D, showed that genes involved in "collagen degradation," "activation of matrix metalloproteases," or "degradation of the extracellular matrix" were upregulated (positive $\log_2$-fold-changes) in the day-10 DMSO-treated cells compared with day-3 DMSO-treated cells. On the other hand, genes involved in the innate immune system seemed to be down-regulated in day-10 DMSO-treated cells.

Then a pairwise comparison between diuron-treated and DMSO-treated cells at day 10 was performed, and significantly differentially expressed genes (Figure 4E; Excel Table S26) were used to do ORA against GO:BP gene sets. In Figure 4F, for the sake of readability, among the significantly overrepresented gene sets, those that are related to osteoclasts function or development are plotted. We can point out "collagen metabolic process," "tissue remodeling," and "glycosaminoglycan catabolic process" among them.

Targets of Osteoclasts Pro-Differentiation Super-Enhancers after Diuron Exposure

To summarize the effect of diuron exposure on key genes driving osteoclastogenesis, the sets of genes differentially expressed in diuron-exposed osteoclasts (Figure 4A) and those targeted by gained super-enhancers (Figure 2A; Figure S7) during normal differentiation were compared. Excel Table S25 presents the list of diuron-affected genes, whereas Excel Tables S12 and S13 provide the lists of targets of gained super-enhancers. *FOSL2*, *CSPG4*, *FAM83G*, *TMEM132A*, *HYOU1*, *VWA1*, *LIF, PRKCH*, *SEMA4D*, *SLC9B1,* and *SLC9B2* were all differentially expressed in diuron-exposed cells and induced by gained super-enhancers that showed significant higher enrichment in H3K27ac at day 10 compared with day-3 undifferentiated cells, whereas *FOSL2*, *CSPG4, PLEKH1*, *VWA1*, *ATP6V1E1*, *LIF*, *JDP2*, *MMP9*, *NFATC1*, *SEMA4D,* and *N4BP2* were differentially expressed in diuron-exposed cells and induced by super-enhancers that were increased significantly at day 7. A Fisher's exact test was performed comparing super-enhancer–associated genes at day 10 (Excel Table S13) and those identified as diuron-affected genes (Excel Table S25). The total number of genes was restricted to genes of Genecode's GRCh37 (version 35) gene annotation file expressed (normalized read counts >20) in at least one sample. The test gives a significant enrichment and an odds ratio (OR) with 95% confidence interval (CI) of >2.7 (Table 1). This suggests an enrichment of genes induced by gained super-enhancers during differentiation among the diuron-affected genes. To express it differently, these results suggest that 0.54% of genes were regulated by gained super-enhancers during osteoclast differentiation, whereas 2.5% of diuron-affected genes were regulated by gained super-enhancer, so they were about 5-fold enriched.

The OR was even higher when the test was performed on the list of high-confidence associations, meaning those that also displayed linkage between the enhancers and the surrounding genes through evolution. Fifty-five of the 122 targets of gained super-enhancers we identified displayed evolutionarily conserved linkage as observed by PEGASUS. Interestingly, 10 of the 11 target genes [except von Willebrand factor A (*VWA*)] that were identified as targets of gained super-enhancers and were differentially expressed in diuron-exposed MSCs were part of the high-confidence list cross-validated with PEGASUS. Fisher's exact test with these numbers gave an OR of 11.45 (95% CI: 5.11, 23.24) and a $p = 9.23 \times 10^{-8}$.

Interestingly, all 11 genes that were differentially expressed after diuron treatment in MSCs among those identified as induced by all differentially active super-enhancers (lost and gained super-enhancer) during the differentiation process, were targets of gained super-enhancers and none of lost super-enhancers.

Discussion

Bone homeostasis is a very tightly regulated process involving a balance between osteoblastic and osteoclastic activities.[61] This balance is based on cell interactions but also on the higher regulated differentiation of osteoblasts and osteoclasts, implicating the orchestration of a complex transcriptional network. It has already been demonstrated numerous times that epigenetic regulations are implicated in the osteoclast differentiation and resorption activity.[62–65]

Corroborating these reports, our study suggests that key osteoclastic genes seem to be induced by newly acquired super-enhancers during osteoclast formation. *FOSL2* and *JDP2* can be mentioned within this context, such that gained super-enhancers within the vicinity of these genes seem to be activated in the late days of differentiation. The role of JDP2 in osteoclastogenesis is already described.[66] Similarly, FOSL2 and LIF/LIFR pathways were also reported to play an important role in regulating osteoclastogenesis.[67] *CXCR1* gene expression also seems to be induced by a gained super-enhancer. In this study, we made the observation that the herbicide diuron has the potential to interfere with the transcriptional program, leading to osteoclast differentiation, even at relatively low concentrations relative to those used in other *in vitro* studies.[22]

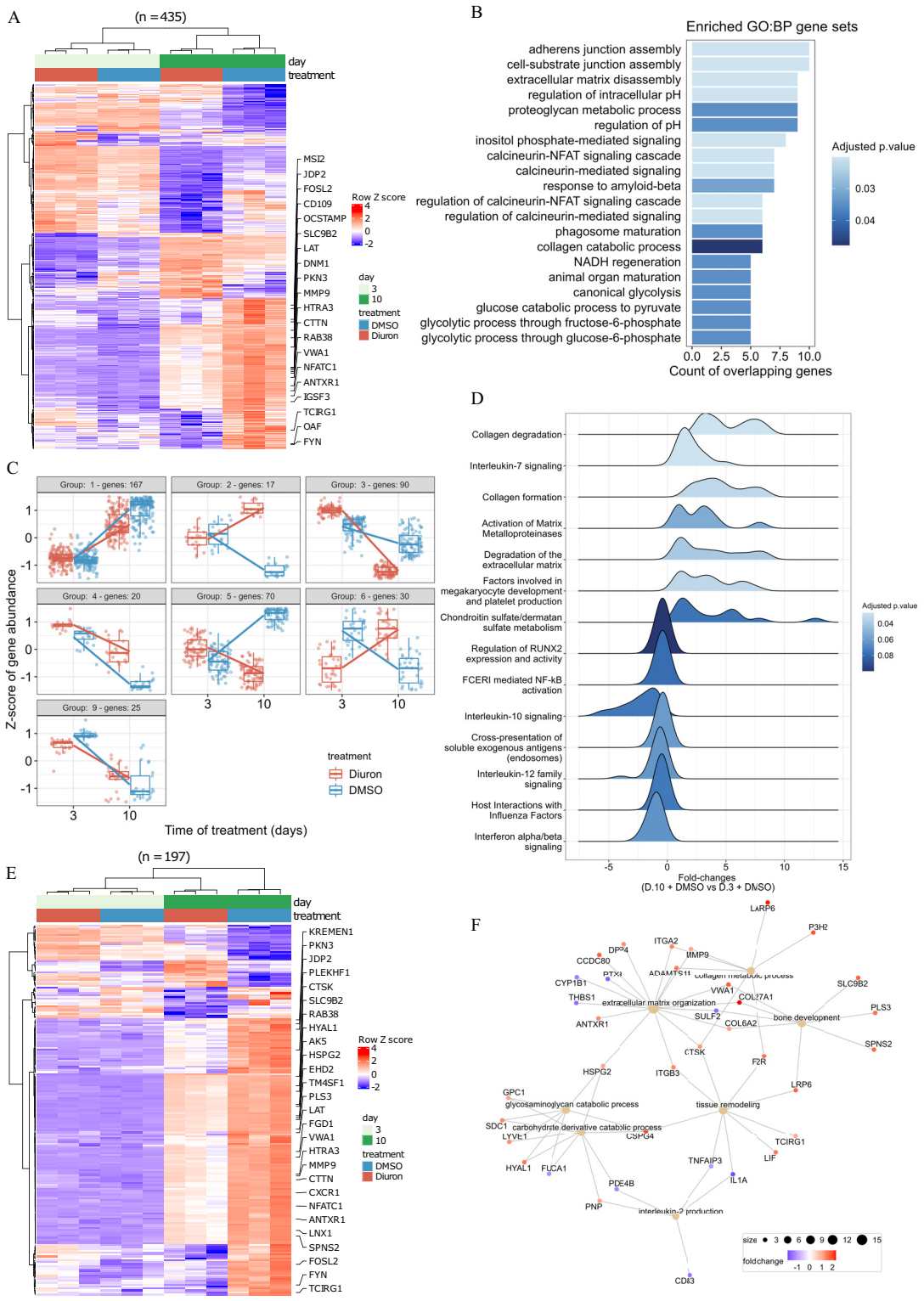

Figure 4. Osteoclast differentiation transcriptional profile during 10 μM diuron exposure. $CD14^+$ premonocytes were treated with differentiation medium and either DMSO or diuron at 10 μM. Cells were harvested for RNA-Seq at day 3 or day 10 of differentiation. To identify differentially expressed genes, an LRT was performed to take into consideration both the effects time and treatment, and the Wald test was performed for pairwise comparisons. (A) Relative expression of significantly differentially expressed genes in LRT (full model: time + treatment + time:treatment vs. reduced model: time + treatment, $p < 0.05$; Excel Table S25 provides z-score values underlying the heatmap). (B) Top overrepresented GO:BP terms in the list of genes from (A). (C) z-Scores of gene abundance in different clusters of genes from A. (D) Summary of GSEA results on pairwise Wald test of day-10 DMSO vs. day-3 DMSO; on the x-axis are the $\log_2$-fold-changes. (E) Relative expressions of significantly differentially expressed genes in Wald pairwise between day-10 DMSO and day-10 diuron (z-score values underlying heatmap are in Excel Table S26). (F) Representation of some of the overrepresented gene sets that are related to osteoclasts function (with keywords: bone remodeling, extracellular matrix, osteoclast) and $\log_2$-fold-changes (DMSO day 10/diuron day 10) of member genes from (E). Note: DMSO, dimethyl sulfoxide; GO:BP, Gene Onotology's Biological Processes; GSEA, gene set enrichment analysis; LRT, likelihood-ratio test; RNA-Seq, RNA-sequencing.

Our observations also associated *CD93* to a super-enhancer that is lost during the course of osteoclastic differentiation. Interestingly, down-regulation of *Cd93* gene expression was reported to increase osteoclastogenesis in a murine model.[68]

To go deeper into the interpretation of the RNA-Seq, some observations should be mentioned. Among the genes identified through RNA-Seq, *CALCR*, *JDP2*, *TCIRG1,* and *ACP5* seemed highly specific to osteoclast differentiations. *DCSTAMP* seemed to be induced even without differentiation medium, so it is not specific enough to verify full maturation of osteoclasts.

The AP-1 family transcription factor FOS, described as playing a key role in osteoclastogenesis,[4] was not significantly differentially expressed in this model; however, significantly higher expression of *FOSL2* and *JDP2* were observed and their expression was accompanied by a higher expression of their potential respective super-enhancers.

Interestingly, the CXCR1 receptor to interleukin-8 seemed to be highly induced at day 7, and its high expression was maintained up to day 10. This induction seemed also to be supported with a gained super-enhancer associated with our approach at day 10. Even though the role of CXCR1 based on its expression level during differentiation process seems to be controversial, our observations suggest a pro-osteoclastogenesis role for CXCR1.[69–71] Regarding DNM1, it has been described as playing an important role in multinucleation in osteoclasts.[72] Among the genes activated during osteoclast differentiation, we identified the ones under the regulation of super-enhancers. It is very interesting to note that the transcripts that were identified as differentially expressed in diuron-treated osteoclasts compared with control cells were enriched within this group of super-enhancers–controlled genes. Study of enhancers and super-enhancers requires an appropriate annotation of identified enhancers, namely, target genes assignment.

Indeed, enhancer annotation raises some challenges owing to the particular characteristics of these elements. Among these characteristics, we can mention their ability to target genes located hundreds of kilobases upstream or downstream.[73] Nevertheless, based on the current understanding of genome organization and admitting that enhancers activity requires chromatin looping, their targets could only be located within their TADs. These domains, conserved among tissues and genomes, gather coregulated regulatory elements and genes, creating a microenvironment within which intergenomic interactions are highly frequent.[45,74] We also observed a discrepancy between the activation of enhancers/super-enhancers and the expression of their associated target genes when considering proliferation medium–treated cells. Our observations lead us to conclude that even though the super-enhancers seemed active, they lacked efficiency in the regulation of their target genes. The lack of up-regulation of genes encoding for transcription factors, such as *NFATC1, FOSL2,* and *JDP2,* in the proliferation medium–treated cells could suggest a reduced recruitment of these effector proteins within the enhancer/super-enhancer regions, meaning accessible chromatin is not sufficient.

Even though mutations in enhancers are associated with developmental disorders, resulting in a higher sequence conservation compared with other noncoding elements, they evolve relatively fast when compared with tissue-specific gene expression patterns.[75,76] This faster evolution rate in enhancers could be explained by mutations in reshuffling of TFs binding sites that have no functional consequences and enhancers' functional redundancy, which dampens mutations' effects, among other reasons. When compared with the PEGASUS database, we observed a high rate of CNEs in the active super-enhancers. We also observed a fairly high (40%–60%) conservation of synteny between our super-enhancers and the genes to which we associated them. These observations support our strategy of identification of functional active super-enhancers and their associated target genes via H3K27ac ChIP-sequencing.

Given that the target genes of the super-enhancers identified in our model are potential key genes leading to osteoclast differentiation, there is a possibility that their preferential mys-regulation by an external factor, such as diuron, could affect osteoclast maturation and function. Short-term diuron treatment might help to identify direct short-term effects.

We make the hypothesis of an epigenetic influence of diuron, at least partially, on osteoclast development through the deregulation of the super-enhancers. Overall, our study shed light on the negative effect of the herbicide diuron on osteoclast differentiation and on osteoblast survival and would justify the use of an *in vivo* model to assess bone parameters in the presence of such compounds before its commercial usage. Our study on cell systems with relatively low concentrations of diuron, compared with studies in animal models, has allowed us to characterize subtle alterations on cells epigenome or identity. These subtle effects could result in major phenotypic consequences over time owing to long-term and cumulative exposure, hence the relevance to evaluating compounds' toxicity on cell systems rather than exclusively on animal models.

Acknowledgments

The authors give special thanks to V. Boeva, who proofread the manuscript and gave suggestions on adding some supplementary figures. The authors are also grateful to A. Postec and M. Dupuy for their assistance during the reviewing process.

This work was supported by the Région Pays de la loire, Episavmen consortium, and Nantes University, Agence Nationale de la Recherche (ANR) Epibone.

RNA-sequencing and ChIP-sequencing data are accessible on the National Center for Biotechnology Information Gene Expression Omnibus Database under the accession code GSE178196.

Normalized bigWig tracks of ChIP-Seq data are available for visualization on the University of California, Santa Cruz, Genome Browser in a saved session (http://genome-euro.ucsc.edu/s/epistressLab/final_hg19_effect_diuron_oc).

R scripts for analysis of RNA-Seq and ChIP-Seq data are available on GitHub (https://github.com/EpistressLab/OC_diuron_paper).

References

1. Boyle WJ, Simonet WS, Lacey DL. 2003. Osteoclast differentiation and activation. Nature 423(6937):337–342, PMID: 12748652, https://doi.org/10.1038/nature01658.
2. Rodan GA, Martin TJ. 2000. Therapeutic approaches to bone diseases. Science 289(5484):1508–1514, PMID: 10968781, https://doi.org/10.1126/science.289.5484.1508.
3. Lamoureux F, Baud'huin M, Rodriguez Calleja L, Jacques C, Berreur M, Rédini F, et al. 2014. Selective inhibition of BET bromodomain epigenetic signalling interferes with the bone-associated tumour vicious cycle. Nat Commun 5:3511, PMID: 24646477, https://doi.org/10.1038/ncomms4511.
4. Park JH, Lee NK, Lee SY. 2017. Current understanding of RANK signaling in osteoclast differentiation and maturation. Mol Cells 40(10):706–713, PMID: 29047262, https://doi.org/10.14348/molcells.2017.0225.
5. Frattini A, Orchard PJ, Sobacchi C, Giliani S, Abinun M, Mattsson JP, et al. 2000. Defects in TCIRG1 subunit of the vacuolar proton pump are responsible for a subset of human autosomal recessive osteopetrosis. Nat Genet 25(3):343–346, PMID: 10888887, https://doi.org/10.1038/77131.
6. Lacey DL, Timms E, Tan HL, Kelley MJ, Dunstan CR, Burgess T, et al. 1998. Osteoprotegerin ligand is a cytokine that regulates osteoclast differentiation and activation. Cell 93(2):165–176, PMID: 9568710, https://doi.org/10.1016/s0092-8674(00)81569-x.
7. Hnisz D, Schuijers J, Lin CY, Weintraub AS, Abraham BJ, Lee TI, et al. 2015. Convergence of developmental and oncogenic signaling pathways at transcriptional super-enhancers. Mol Cell 58(2):362–370, PMID: 25801169, https://doi.org/10.1016/j.molcel.2015.02.014.
8. Pott S, Lieb JD. 2015. What are super-enhancers? Nat Genet 47(1):8–12, PMID: 25547603, https://doi.org/10.1038/ng.3167.

9. Whyte WA, Orlando DA, Hnisz D, Abraham BJ, Lin CY, Kagey MH, et al. 2013. Master transcription factors and mediator establish super-enhancers at key cell identity genes. Cell 153(2):307–319, PMID: 23582322, https://doi.org/10.1016/j.cell.2013.03.035.
10. Lee BK, Jang YJ, Kim M, LeBlanc L, Rhee C, Lee J, et al. 2019. Super-enhancer-guided mapping of regulatory networks controlling mouse trophoblast stem cells. Nat Commun 10(1):4749, PMID: 31628347, https://doi.org/10.1038/s41467-019-12720-6.
11. Ministère de l'agriculture et de la pêche. 2008. Avis aux fabricants, distributeurs et utilisateurs de produits phytopharmaceutiques concernant le retrait des préparations contenant des substances actives considérées comme dangereuses et les délais d'écoulement octroyés pour leur distribution et leur utilisation. Journal Officiel De La République Française. Text No. 142 of 161. https://www.legifrance.gouv.fr/jorf/id/JORFTEXT000018453651 [accessed 8 April 2023].
12. Hope BK, Pillsbury L, Boling B. 2012. A state-wide survey in Oregon (USA) of trace metals and organic chemicals in municipal effluent. Sci Total Environ 417–418:263–272, PMID: 22244355, https://doi.org/10.1016/j.scitotenv.2011.12.028.
13. Köck-Schulmeyer M, Ginebreda A, González S, Cortina JL, de Alda ML, Barceló D. 2012. Analysis of the occurrence and risk assessment of polar pesticides in the Llobregat River Basin (NE Spain). Chemosphere 86(1):8–16, PMID: 21925700, https://doi.org/10.1016/j.chemosphere.2011.08.034.
14. Barizon RRM, Figueiredo RO, de Souza Dutra DRC, Regitano JB, Ferracini VL. 2020. Pesticides in the surface waters of the Camanducaia River watershed, Brazil. J Environ Sci Health B 55(3):283–292, PMID: 31778093, https://doi.org/10.1080/03601234.2019.1693835.
15. European Chemicals Agency. n.d. Diuron (ISO); 3-(3,4-dichlorophenyl)-1,1-dimethylurea. EC number: 206-354-4. https://echa.europa.eu/registration-dossier/-/registered-dossier/13520/2/1 [accessed 8 April 2023].
16. Taylor LL, Rinde E. 1997. Memorandum: Carcinogenicity peer review of diuron. From Linda L. Taylor, Review Section II, Toxicology Branch II, Health Effects Division and Esther Rinde, Manager, Carcinogenicity Peer Review, Science Analysis Branch, Health Effects Division, U.S. Environmental Protection Agency through Stephanie R. Irene, Deputy Director, Health Effects Division to Philip Errico, Product Manager #25, Fungicide-Herbicide Branch, Registration Division (7505C) and Larry Schnaubelt, Special Review and Reregistration Division (7508W). Published online May 8. https://www3.epa.gov/pesticides/chem_search/cleared_reviews/csr_PC-035505_8-May-97_042.pdf [accessed 4 October 2023].
17. Gallo A, Tosti E. 2013. Adverse effect of antifouling compounds on the reproductive mechanisms of the ascidian *Ciona intestinalis*. Mar Drugs 11(9):3554–3568, PMID: 24065165, https://doi.org/10.3390/md11093554.
18. Pereira TSB, Boscolo CNP, da Silva DGH, Batlouni SR, Schlenk D, de Almeida EA. 2015. Anti-androgenic activities of diuron and its metabolites in male Nile tilapia (*Oreochromis niloticus*). Aquat Toxicol 164:10–15, PMID: 25930013, https://doi.org/10.1016/j.aquatox.2015.04.013.
19. Pereira TSB, Boscolo CNP, Felício AA, Batlouni SR, Schlenk D, de Almeida EA. 2016. Estrogenic activities of diuron metabolites in female Nile tilapia (*Oreochromis niloticus*). Chemosphere 146:497–502, PMID: 26741556, https://doi.org/10.1016/j.chemosphere.2015.12.073.
20. Huovinen M, Loikkanen J, Naarala J, Vähäkangas K. 2015. Toxicity of diuron in human cancer cells. Toxicol In Vitro 29(7):1577–1586, PMID: 26086120, https://doi.org/10.1016/j.tiv.2015.06.013.
21. Iyer P, V. Alexeeff G, Zeise L, Donald JM, Robinson N, Emery L. 2002. *Evidence on the Developmental and Reproductive Toxicity of Diuron—Draft. September 2002*. https://oehha.ca.gov/media/downloads/crnr/diuronhid.pdf [accessed 21 November 2022].
22. Briand J, Nadaradjane A, Bougras-Cartron G, Olivier C, Vallette FM, Cartron PF. 2019. Diuron exposure and Akt overexpression promote glioma formation through DNA hypomethylation. Clin Epigenetics 11(1):159, PMID: 31727122, https://doi.org/10.1186/s13148-019-0759-1.
23. Domingues A, Grassi TF, Spinardi-Barbisan ALT, Barbisan LF. 2012. Developmental exposure to diuron causes splenotoxicity in male Sprague-Dawley rat pups. J Environ Sci Health B 47(5):420–426, PMID: 22424067, https://doi.org/10.1080/03601234.2012.657054.
24. Khera KS, Whalen C, Trivett G, Angers G. 1979. Teratogenicity studies on pesticidal formulations of dimethoate, diuron and lindane in rats. Bull Environ Contam Toxicol 22(4–5):522–529, PMID: 90533, https://doi.org/10.1007/BF02026981.
25. Fekete N, Rojewski MT, Fürst D, Kreja L, Ignatius A, Dausend J, et al. 2012. GMP-compliant isolation and large-scale expansion of bone marrow-derived MSC. PLoS One 7(8):e43255, PMID: 22905242, https://doi.org/10.1371/journal.pone.0043255.
26. Rojewski MT, Lotfi R, Gjerde C, Mustafa K, Veronesi E, Ahmed AB, et al. 2019. Translation of a standardized manufacturing protocol for mesenchymal stromal cells: a systematic comparison of validation and manufacturing data. Cytotherapy 21(4):468–482, PMID: 30926359, https://doi.org/10.1016/j.jcyt.2019.03.001.
27. Duplomb L, Baud'huin M, Charrier C, Berreur M, Trichet V, Blanchard F, et al. 2008. Interleukin-6 inhibits receptor activator of nuclear factor κB ligand-induced osteoclastogenesis by diverting cells into the macrophage lineage: key role of Serine727 phosphorylation of signal transducer and activator of transcription 3. Endocrinology 149(7):3688–3697, PMID: 18403479, https://doi.org/10.1210/en.2007-1719.
28. Schneider CA, Rasband WS, Eliceiri KW. 2012. NIH image to ImageJ: 25 years of image analysis. Nat Methods 9(7):671–675, PMID: 22930834, https://doi.org/10.1038/nmeth.2089.
29. van Galen P, Viny AD, Ram O, Ryan RJH, Cotton MJ, Donohue L, et al. 2016. A multiplexed system for quantitative comparisons of chromatin landscapes. Mol Cell 61(1):170–180, PMID: 26687680, https://doi.org/10.1016/j.molcel.2015.11.003.
30. Li H. 2013. Aligning sequence reads, clone sequences and assembly contigs with BWA-MEM. ArXiv. 13033997. Preprint posted online March 15, 2013, https://doi.org/10.48550/arXiv.1303.3997.
31. Zhang Y, Liu T, Meyer CA, Eeckhoute J, Johnson DS, Bernstein BE, et al. 2008. Model-based Analysis of ChIP-Seq (MACS). Genome Biol 9(9):R137, PMID: 18798982, https://doi.org/10.1186/gb-2008-9-9-r137.
32. Leimbach A. 2016. bac-genomics-scripts: bovine E. coli mastitis comparative genomics edition (bovine_ecoli_mastitis). Zenodo. Published online December 21, 2016. https://doi.org/10.5281/zenodo.215824.
33. Chen S, Zhou Y, Chen Y, Gu J. 2018. fastp: an ultra-fast all-in-one FASTQ preprocessor. Bioinformatics 34(17):i884–i890, PMID: 30423086, https://doi.org/10.1093/bioinformatics/bty560.
34. Kim D, Paggi JM, Park C, Bennett C, Salzberg SL. 2019. Graph-based genome alignment and genotyping with HISAT2 and HISAT-genotype. Nat Biotechnol 37(8):907–915, PMID: 31375807, https://doi.org/10.1038/s41587-019-0201-4.
35. Kovaka S, Zimin AV, Pertea GM, Razaghi R, Salzberg SL, Pertea M. 2019. Transcriptome assembly from long-read RNA-seq alignments with StringTie2. Genome Biol 20(1):278, PMID: 31842956, https://doi.org/10.1186/s13059-019-1910-1.
36. Love MI, Huber W, Anders S. 2014. Moderated estimation of fold change and dispersion for RNA-seq data with DESeq2. Genome Biol 15(12):550, PMID: 25516281, https://doi.org/10.1186/s13059-014-0550-8.
37. Yu G, Wang LG, Han Y, He QY. 2012. clusterProfiler: an R package for comparing biological themes among gene clusters. OMICS 16(5):284–287, PMID: 22455463, https://doi.org/10.1089/omi.2011.0118.
38. Yu G, He QY. 2016. ReactomePA: an R/Bioconductor package for reactome pathway analysis and visualization. Mol Biosyst 12(2):477–479, PMID: 26661513, https://doi.org/10.1039/c5mb00663e.
39. Love M. 2023. Package 'DESeq2'. Differential gene expression analysis based on the negative binominal distribution. Version 1.41.1. https://bioconductor.org/packages/devel/bioc/manuals/DESeq2/man/DESeq2.pdf [accessed 31 May 2023].
40. Lovén J, Hoke HA, Lin CY, Lau A, Orlando DA, Vakoc CR, et al. 2013. Selective inhibition of tumor oncogenes by disruption of super-enhancers. Cell 153(2):320–334, PMID: 23582323, https://doi.org/10.1016/j.cell.2013.03.036.
41. Liao Y, Smyth GK, Shi W. 2019. The R package *Rsubread* is easier, faster, cheaper and better for alignment and quantification of RNA sequencing reads. Nucleic Acids Res 47(8):e47, PMID: 30783653, https://doi.org/10.1093/nar/gkz114.
42. Risso D, Schwartz K, Sherlock G, Dudoit S. 2011. GC-content normalization for RNA-Seq data. BMC Bioinformatics 12(1):480, PMID: 22177264, https://doi.org/10.1186/1471-2105-12-480.
43. Ott CJ, Federation AJ, Schwartz LS, Kasar S, Klitgaard JL, Lenci R, et al. 2018. Enhancer architecture and essential core regulatory circuitry of chronic lymphocytic leukemia. Cancer Cell 34(6):982–995.e7, PMID: 30503705, https://doi.org/10.1016/j.ccell.2018.11.001.
44. Ramírez F, Ryan DP, Grüning B, Bhardwaj V, Kilpert F, Richter AS, et al. 2016. deepTools2: a next generation web server for deep-sequencing data analysis. Nucleic Acids Res 44(W1):W160–W165, PMID: 27079975, https://doi.org/10.1093/nar/gkw257.
45. Dixon JR, Jung I, Selvaraj S, Shen Y, Antosiewicz-Bourget JE, Lee AY, et al. 2015. Chromatin architecture reorganization during stem cell differentiation. Nature 518(7539):331–336, PMID: 25693564, https://doi.org/10.1038/nature14222.
46. Dixon JR, Selvaraj S, Yue F, Kim A, Li Y, Shen Y, et al. 2012. Topological domains in mammalian genomes identified by analysis of chromatin interactions. Nature 485(7398):376–380, PMID: 22495300, https://doi.org/10.1038/nature11082.
47. Sexton T, Yaffe E, Kenigsberg E, Bantignies F, Leblanc B, Hoichman M, et al. 2012. Three-dimensional folding and functional organization principles of the *Drosophila* genome. Cell 148(3):458–472, PMID: 22265598, https://doi.org/10.1016/j.cell.2012.01.010.
48. Nora EP, Lajoie BR, Schulz EG, Giorgetti L, Okamoto I, Servant N, et al. 2012. Spatial partitioning of the regulatory landscape of the X-inactivation

centre. Nature 485(7398):381–385, PMID: 22495304, https://doi.org/10.1038/nature11049.
49. Lieberman-Aiden E, van Berkum NL, Williams L, Imakaev M, Ragoczy T, Telling A, et al. 2009. Comprehensive mapping of long range interactions reveals folding principles of the human genome. Science 326(5950):289–293, PMID: 19815776, https://doi.org/10.1126/science.1181369.
50. Dowen JM, Fan ZP, Hnisz D, Ren G, Abraham BJ, Zhang LN, et al. 2014. Control of cell identity genes occurs in insulated neighborhoods in mammalian chromosomes. Cell 159(2):374–387, PMID: 25303531, https://doi.org/10.1016/j.cell.2014.09.030.
51. McLeay RC, Bailey TL. 2010. Motif enrichment analysis: a unified framework and an evaluation on ChIP data. BMC Bioinformatics 11(1):165, PMID: 20356413, https://doi.org/10.1186/1471-2105-11-165.
52. Creyghton MP, Cheng AW, Welstead GG, Kooistra T, Carey BW, Steine EJ, et al. 2010. Histone H3K27ac separates active from poised enhancers and predicts developmental state. Proc Natl Acad Sci USA 107(50):21931–21936, PMID: 21106759, https://doi.org/10.1073/pnas.1016071107.
53. Karlić R, Chung HR, Lasserre J, Vlahoviček K, Vingron M. 2010. Histone modification levels are predictive for gene expression. Proc Natl Acad Sci USA 107(7):2926–2931, PMID: 20133639, https://doi.org/10.1073/pnas.0909344107.
54. Naville M, Ishibashi M, Ferg M, Bengani H, Rinkwitz S, Krecsmarik M, et al. 2015. Long-range evolutionary constraints reveal *cis*-regulatory interactions on the human X chromosome. Nat Commun 6(1):6904, PMID: 25908307, https://doi.org/10.1038/ncomms7904.
55. Clément Y, Torbey P, Gilardi-Hebenstreit P, Roest Crollius H. 2020. Enhancer–gene maps in the human and zebrafish genomes using evolutionary linkage conservation. Nucleic Acids Res 48(5):2357–2371, PMID: 31943068, https://doi.org/10.1093/nar/gkz1199.
56. Engsig MT, Chen QJ, Vu TH, Pedersen AC, Therkidsen B, Lund LR, et al. 2000. Matrix metalloproteinase 9 and vascular endothelial growth factor are essential for osteoclast recruitment into developing long bones. J Cell Biol 151(4):879–889, PMID: 11076971, https://doi.org/10.1083/jcb.151.4.879.
57. Yu X, Huang Y, Collin-Osdoby P, Osdoby P. 2003. Stromal cell-derived factor-1 (SDF-1) recruits osteoclast precursors by inducing chemotaxis, matrix metalloproteinase-9 (MMP-9) activity, and collagen transmigration. J Bone Miner Res 18(8):1404–1418, PMID: 12929930, https://doi.org/10.1359/jbmr.2003.18.8.1404.
58. Yang M, Birnbaum MJ, MacKay CA, Mason-Savas A, Thompson B, Odgren PR. 2008. Osteoclast stimulatory transmembrane protein (OC-STAMP), a novel protein induced by RANKL that promotes osteoclast differentiation. J Cell Physiol 215(2):497–505, PMID: 18064667, https://doi.org/10.1002/jcp.21331.
59. Winslow MM, Pan M, Starbuck M, Gallo EM, Deng L, Karsenty G, et al. 2006. Calcineurin/NFAT signaling in osteoblasts regulates bone mass. Dev Cell 10(6):771–782, PMID: 16740479, https://doi.org/10.1016/j.devcel.2006.04.006.
60. Pantano L, Hutchinson J, Barrera V, Piper M, Khetani R, Daily K, et al. 2020. DEGreport: Report of DEG analysis. Bioconductor. https://doi.org/10.18129/B9.bioc.DEGreport.
61. Al-Bari AA, Al Mamun A. 2020. Current advances in regulation of bone homeostasis. FASEB Bioadv 2(11):668–679, PMID: 33205007, https://doi.org/10.1096/fba.2020-00058.
62. Caputo VS, Trasanidis N, Xiao X, Robinson ME, Katsarou A, Ponnusamy K, et al. 2021. Brd2/4 and Myc regulate alternative cell lineage programmes during early osteoclast differentiation in vitro. iScience 24(1):101989, PMID: 33490899, https://doi.org/10.1016/j.isci.2020.101989.
63. Lee S, Kim HS, Kim MJ, Min KY, Choi WS, You JS. 2021. Glutamine metabolite α-ketoglutarate acts as an epigenetic co-factor to interfere with osteoclast differentiation. Bone 145:115836, PMID: 33383217, https://doi.org/10.1016/j.bone.2020.115836.
64. Jacques C, Lavaud M, Georges S, Tesfaye R, Baud'huin M, Lamoureux F, et al. 2020. BET bromodomains' functions in bone-related pathologies. Epigenomics 12(2):127–144, PMID: 31849242, https://doi.org/10.2217/epi-2019-0172.
65. Baud'huin M, Lamoureux F, Jacques C, Rodriguez Calleja L, Quillard T, Charrier C, et al. 2017. Inhibition of BET proteins and epigenetic signaling as a potential treatment for osteoporosis. Bone 94:10–21, PMID: 27669656, https://doi.org/10.1016/j.bone.2016.09.020.
66. Maruyama K, Fukasaka M, Vandenbon A, Saitoh T, Kawasaki T, Kondo T, et al. 2012. The transcription factor Jdp2 controls bone homeostasis and antibacterial immunity by regulating osteoclast and neutrophil differentiation. Immunity 37(6):1024–1036, PMID: 23200825, https://doi.org/10.1016/j.immuni.2012.08.022.
67. Bozec A, Bakiri L, Hoebertz A, Eferl R, Schilling AF, Komnenovic V, et al. 2008. Osteoclast size is controlled by Fra-2 through LIF/LIF-receptor signalling and hypoxia. Nature 454(7201):221–225, PMID: 18548006, https://doi.org/10.1038/nature07019.
68. Franceschetti T, Kessler CB, Lee SK, Delany AM. 2013. miR-29 promotes murine osteoclastogenesis by regulating osteoclast commitment and migration. J Biol Chem 288(46):33347–33360, PMID: 24085298, https://doi.org/10.1074/jbc.M113.484568.
69. Bendre MS, Montague DC, Peery T, Akel NS, Gaddy D, Suva LJ. 2003. Interleukin-8 stimulation of osteoclastogenesis and bone resorption is a mechanism for the increased osteolysis of metastatic bone disease. Bone 33(1):28–37, PMID: 12919697, https://doi.org/10.1016/s8756-3282(03)00086-3.
70. Grassi F, Piacentini A, Cristino S, Toneguzzi S, Cavallo C, Facchini A, et al. 2003. Human osteoclasts express different CXC chemokines depending on cell culture substrate: molecular and immunocytochemical evidence of high levels of CXCL10 and CXCL12. Histochem Cell Biol 120(5):391–400, PMID: 14600836, https://doi.org/10.1007/s00418-003-0587-3.
71. Kopesky P, Tiedemann K, Alkekhia D, Zechner C, Millard B, Schoeberl B, et al. 2014. Autocrine signaling is a key regulatory element during osteoclastogenesis. Biol Open 3(8):767–776, PMID: 25063197, https://doi.org/10.1242/bio.20148128.
72. Shin NY, Choi H, Neff L, Wu Y, Saito H, Ferguson SM, et al. 2014. Dynamin and endocytosis are required for the fusion of osteoclasts and myoblasts. J Cell Biol 207(1):73–89, PMID: 25287300, https://doi.org/10.1083/jcb.201401137.
73. Tolhuis B, Palstra RJ, Splinter E, Grosveld F, de Laat W. 2002. Looping and interaction between hypersensitive sites in the active β-globin locus. Mol Cell 10(6):1453–1465, PMID: 12504019, https://doi.org/10.1016/s1097-2765(02)00781-5.
74. Rao SSP, Huntley MH, Durand NC, Stamenova EK, Bochkov ID, Robinson JT, et al. 2014. A 3D map of the human genome at kilobase resolution reveals principles of chromatin looping. Cell 159(7):1665–1680, PMID: 25497547, https://doi.org/10.1016/j.cell.2014.11.021.
75. Merkin J, Russell C, Chen P, Burge CB. 2012. Evolutionary dynamics of gene and isoform regulation in mammalian tissues. Science 338(6114):1593–1599, PMID: 23258891, https://doi.org/10.1126/science.1228186.
76. Blow MJ, McCulley DJ, Li Z, Zhang T, Akiyama JA, Holt A, et al. 2010. ChIP-Seq identification of weakly conserved heart enhancers. Nat Genet 42(9):806–810, PMID: 20729851, https://doi.org/10.1038/ng.650.